Instantaneous frequency measurement for IR-UWB signal in CMOS 130 nm

A. Goavec, Remy Vauche, Jean Gaubert, F. Hameau, M. Zarudniev, Eric Mercier

Instantaneous Frequency Measurement for IR-UWB signal in CMOS 130 nm

A. Goavec, R. Vauché, J. Gaubert
Aix-Marseille Université, CNRS, Université de Toulon
IM2NP UMR 7334
Marseille, France
{anthony.goavec; remy.vauche; jean.gaubert}@univ-amu.fr

A. Goavec, F. Hameau, M. Zarudniev, E. Mercier
Univ. Grenoble Alpes, F-38000 Grenoble, France
CEA, LETI, MINATEC Campus, F-38054
Grenoble, France
{anthony.goavec; frederic.hameau; mykhailo.zarudniev, eric.mercier}@cea.fr

***Abstract*— During the last decade, Ultra-WideBand applications showed many interests for radio and imaging applications in the [3.1-4.9 GHz] frequency band. To realize such applications in other frequency domains, the instantaneous frequency of the impulse signal is commonly used. This paper describes the design of an Instantaneous Frequency Measurement system in order to show the feasibility to use it for Ultra-WideBand impulse radio radar and imaging applications. The integrated part of the system is constituted of a full-wave rectifier, a delay cell and an analog multiplier. These devices was designed in CMOS 130 nm technology and the post-layout simulation are shown in comparison to theoretical Matlab simulations.**

Keywords—Instantaneous Frequency Measurement, Ultra-WideBand, Impulse Radio

I. INTRODUCTION

Since about a decade, Ultra-WideBand (UWB) technology has demonstrated its potential for high and low data rate short range wireless communications [1]. Moreover it has high localization performances by accurate measurement of the time of flight thanks to its robustness to multipath fading. In 2002 the Federal Communications Commission (FCC) defined an UWB signal with a minimum −10 dB bandwidth of 500 MHz or −10 dB fractional bandwidth of 20% [2]. To enable the coexistence and dissemination of UWB systems, the FCC and the European Telecommunications Standards Institute (ETSI) set power emission constraints for all kinds of UWB devices operating in the 3.1 to 10.6 GHz UWB frequency band. Inside the band, the mean power spectrum density is limited to −41.3 dBm/MHz (0 dBm/50 MHz for the peak power spectrum density). In this frequency band, the FCC considers many applications: imaging systems such as ground penetrating radar, surveillance systems to detect the intrusion of persons in a stationary RF perimeter field or medical systems to localize the body of a person or an animal.

Such UWB transceivers have been realized in the [3-5 GHz] frequency band in order to realize such applications. To treat the received data, a common solution is to work on the amplitude or on the energy of the received signal [3]. But for many applications ranging, defense applications as radar and electronic intelligence systems for the determination of unknown signals over a broad band frequency band, Instantaneous Frequency Measurement (IFM) systems are widely used [4] [5]. The concept of instantaneous frequency is very important in the field of time-frequency signal analysis and processing.

The aim of this study is to show the feasibility to measure on-chip the instantaneous frequency of an Impulse Radio (IR) signal in [3.1-4.9 GHz] UWB frequency band. In order to generate a signal with such significant bandwidth, a way is to use impulse modulation instead of carrier modulation since it allows to reduce the complexity and the cost of the transmitter. The Fig. 1 shows the UWB pulse [6] used for this study.

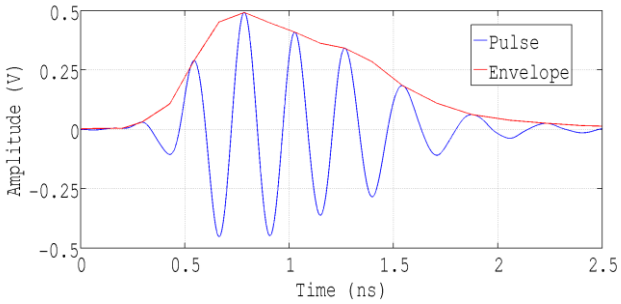

Fig. 1. Example of a pulse in [3.1 – 4.9 GHz] UWB frequency band

Also it is a challenging point to achieve the measure of the instantaneous frequency from this pulse due to its short duration of few nanoseconds combined with the fast evolution of the pulse shape. This paper describes the implementation of the first blocks required to build an IFM receiver in UWB frequency band in order to evaluate future possibilities to use the instantaneous frequency for UWB signal analysis. This paper is organized as follows. In Section II the theoretical method usually exploited for continuous wave signal is presented. In order to implement on-chip this theoretical framework for an IR-UWB signal, the design of integrated devices in 130nm CMOS technology is introduced in the Section III. The simulations results are given in the Section IV and Section V concludes the paper.

II. THEORETICAL METHOD FOR INSTANTANEOUS FREQUENCY MEASUREMENT

In this section two different ways are considered in order to extract the instantaneous frequency from an oscillating signal. The first solution appears in the mathematical expression of the signal. Indeed, the IR-UWB signal in Fig. 1 can be written:

$$s(t) = a(t)\cos\big(2\pi\nu_0 t + \varphi(t)\big). \quad (1)$$

From (1), the function $s(t)$ is actually a finite real envelope $a(t)$ up-converted to the central frequency ν_0 and modulated by the instantaneous phase $\varphi(t)$. By assuming that the instantaneous phase is a differentiable function, it is possible to express the instantaneous frequency as follows:

$$f(t) = \frac{1}{2\pi}\frac{d\varphi}{dt}(t). \quad (2)$$

In view of (1), in order to extract the instantaneous frequency (at least the instantaneous phase), it could be adequate to compute the argument of oscillating cosine wave. However it would necessitate a very expensive cost for the analog-to-digital conversion in terms of silicon area and power consumption. To reduce this cost, a solution could be the use of a local oscillator in order to down-convert the pulse to the baseband frequency. The ideal down-conversion of $s(t)$ using the multiplication by $e^{-j(2\pi\nu_0 t)}$ in time domain gives:

$$s(t)e^{-j(2\pi\nu_0 t)} = \frac{s_{BB}(t) + s_{HRF}(t)}{2}, \quad (3)$$

where

$$s_{BB}(t) = a(t)e^{j\varphi(t)} \quad (4)$$

and

$$s_{HRF}(t) = a(t)e^{-j(2\pi\nu_0 2t + \varphi(t))}. \quad (5)$$

By filtering $s_{HRF}(t)$ all the needed information are contained in the real and the imaginary parts of the baseband signal $s_{BB}(t)$, respectively obtained on I and Q paths (Fig. 2). The box *Arg(.)* in Fig. 2 represents the computation of the angle in Cartesian system thanks to the arctangent function.

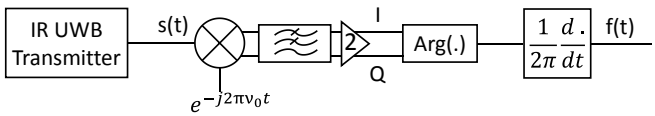

Fig. 2. Estimation of the Instantaneous Frequency with a local oscillator

The measurement of the instantaneous frequency of an oscillating signal shows a great interest for a long time and a lot of techniques exist. A digital instantaneous frequency measurement subsystem was presented in 1996 in [7]. It is based on a mix between the RF signal and the delayed one. This idea is taken again in 2007 in [8] to build a phase-noise measurement circuit. Below the continuous time methods based on the delayed signal, as in [7], is applied to our impulse signal to get the instantaneous frequency.

From the real oscillating signal of (X), a new signal s_τ is built by time delay operation:

$$s_\tau(t) = s(t-\tau) = a(t-\tau)\,cos\big(2\pi\nu_0(t-\tau) + \varphi(t-\tau)\big). \quad (6)$$

The product of s and s_τ gives the mix signal:

$$s_{mix}(t) = \frac{a(t)a(t-\tau)}{2}\big[cos\big(2\pi\nu_0\tau + \varphi(t) - \varphi(t-\tau)\big) + cos\big(2\pi\nu_0(2t-\tau) + \varphi(t) + \varphi(t-\tau)\big)\big]. \quad (7)$$

Then the delay τ is chosen in order to have:

$$2\pi\nu_0\tau = \frac{\pi}{2} + 2k\pi, k \in \mathbb{N}. \quad (8)$$

With the condition (8), due to trigonometric transformation $s_{mix}(t)$ becomes:

$$s_{mix}(t) = -\frac{a(t)a(t-\tau)}{2}\big[\sin\big(\varphi(t) - \varphi(t-\tau)\big) + \sin\big(2\pi\nu_0 2t + \varphi(t) + \varphi(t-\tau)\big)\big]. \quad (9)$$

Here, if the difference $\varphi(t) - \varphi(t-\tau)$ is very close to zero (it means slow variations for the instantaneous phase),

$$\sin\big(\varphi(t) - \varphi(t-\tau)\big) \approx \varphi(t) - \varphi(t-\tau). \quad (10)$$

Combining (9) and (10), the output signal $s_{out}(t)$ of a low-pass filter, used to remove high frequency components, can be divided by the product of the envelope and the delayed envelope. The result is:

$$\frac{s_{out}(t)}{a(t)a(t-\tau)} \approx -\frac{1}{2}\big(\varphi(t) - \varphi(t-\tau)\big). \quad (11)$$

Here, the definition (2) of the instantaneous frequency is not so far. The result in (11) is divided by the delay τ and the estimation gives:

$$f(t) \approx -\frac{1}{a(t)a(t-\tau)}\frac{s_{out}(t)}{\tau\pi}. \quad (12)$$

The Fig. 3 compares the instantaneous frequency obtained in blue with the local oscillator method (according to Fig. 2) and the results computed thanks to (12). The simulations was done here with Matlab. Some differences can be observed between 0.25 and 0.5 ns and after 1.5 ns. These difference are due to the high non-linear behavior of the pulse at its beginning and during its extinction. But on the whole both methods give the same results for the instantaneous frequency. To notice, to compute (12), it was necessary to extract the envelope $a(t)$ of the pulse. For that, the envelope is considered as the linear interpolation between each extremum of the pulse, as shown in red in Fig. 1.

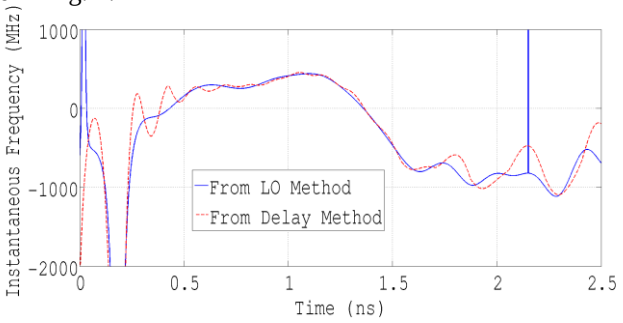

Fig. 3. Comparison with Matlab simulations of Instantaneous Frequency obtained from Fig. 2 operations and with (12)

III. CHIP ARCHITECTURE AND DESIGN

The need of local oscillator to provide the down-converted signal gives lots of constraints for hardware implementation, especially in term of silicon area and power consumption. So in this section the extraction of the instantaneous frequency is implemented according to (12) and the different operations presented in Section II. The system view of the required components is shown in Fig. 4. To notice, the accent of this work is on the feasibility to realize on-chip the extraction of instantaneous frequency for impulse radio signal in the [3.1 – 4.9 GHz] UWB frequency band.

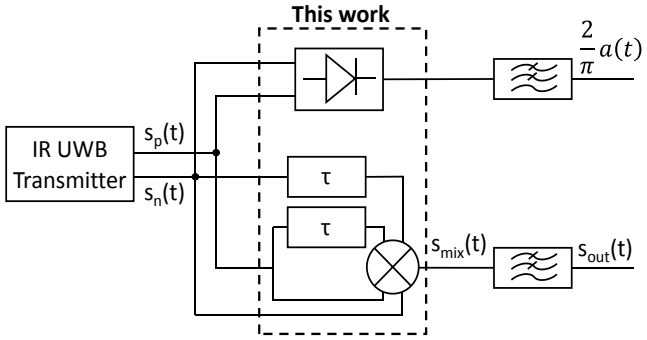

Fig. 4. Estimation of the Instantaneous Frequency

The diode symbolizes a full-wave rectifier implemented in order to extract the envelope of the pulse, necessary to compute the instantaneous frequency according to (12). To realize a first test chip, the low pass filters did not integrate. The transmitter has two outputs with a 180° phase change. It is an advantage in the full-wave rectifier design but it requires two delay cells.

To notice, in the next, each transistor has a length of 130 nm and its width is indicated on the schematic.

A. Full-Wave Rectifier

In order to extract the envelope of the pulse, a full-wave rectifier is used. Indeed, for a T-periodic cosine function with a constant amplitude A, if the wave is fully rectified, its mean value is:

$$< \mathrm{A}\cos\left(\frac{2\pi}{T}t\right) >= \frac{2A}{\pi} \qquad (13)$$

Thus it appears feasible to extract the envelope of the pulse with a full-wave rectifier and a low-pass filter to just keep the mean value of the signal. It is assumed the variations of the envelope a(t) and the instantaneous phase φ(t) do not conflict with (13). In Fig. 5 the schematic view of the full-wave rectifier is shown.

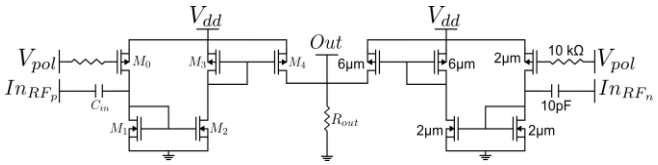

Fig. 5. Schematic of Full-Wave Rectifier

The full-wave rectifier is made of two symmetrical part. Each one removes the negative oscillations [9] from the two outputs of the IR-UWB transmitter which are 180° phase shifted. Indeed, with the transistor M_0 used in current source, the NMOS transistor M_1, connected as a diode, is biased closed to its threshold conductibility. The transistor M_2 constitutes a current mirror with M_1 in order to copy the rectified current. A second current mirror based on PMOS transistors M_3 and M_4 enables to sum the currents from the two sides of the rectifier into the R_{out} resistor in order to have a current to voltage conversion. The C_{in} serie capacitor must be huge in order to reduce the time constant of the low-pass filter resulted in the association of $r_{DS}(M_1)$ and C_{in}.

B. Delay Cells

In order to apply an analog delay, unchanging on the whole frequency band (because it just depends of the carrier frequency ν_0 according to (8)), the design of a first order g_m-C all-pass filter based on [10] was chosen. The Fig. 6 presents the schematic view of the delay cell.

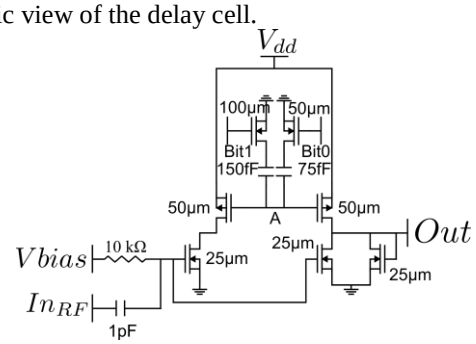

Fig. 6. Schematic of Delay Cell

The delay is given by the ratio between the capacitance on the node A and the transconductance of the transistor PMOS M_4:

$$\tau = \frac{2C}{g_m(M_4)} \qquad (14)$$

Thus in order to be more flexible for testing and to have the possibility to measure pulses with different carrier frequency, a tunable capacitor [11] was built on node A. Thanks to two NMOS RF switches, four values of capacitance will be available.

C. Analog Multiplier

The analog multiplier is based on the work presented in [12]. Two amplification stages in common source were added in order to improve the measurement with greater voltage variations on the output.

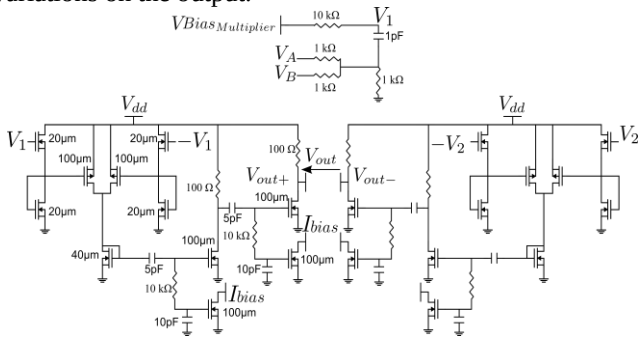

Fig. 7. Schematic of Analog Multiplier

In Fig. 7, the input voltages of the multiplier are:

$$\begin{aligned} V_1 &= s_p(t) + s_p(t-\tau), \\ V_2 &= s_p(t) + s_n(t-\tau), \\ -V_1 &= s_n(t) + s_n(t-\tau), \\ -V_2 &= s_n(t) + s_p(t-\tau). \end{aligned} \qquad (15)$$

Thus four passive resistive voltage adders (only one is shown on Fig. 7) is used in order to generate these voltages.

IV. Post-Layout Simulations Results

In this section the results of post-layout electrical simulations are considered. The devices were designed in HCMOS9 130 nm technology from STMicroelectronics. The low-pass filters have been simulated on Matlab with 3° order Butterworth filters with 1 GHz cut-off frequency.

The Fig. 8 gives the results of the extracted envelope with the full-wave rectifier, compared to linear interpolation from Matlab. Oscillations under the DC component on the output of the rectifier are "lost" thus the envelope is wrong at the beginning and during the extinction. But even if the envelope is overestimated, the results are promising.

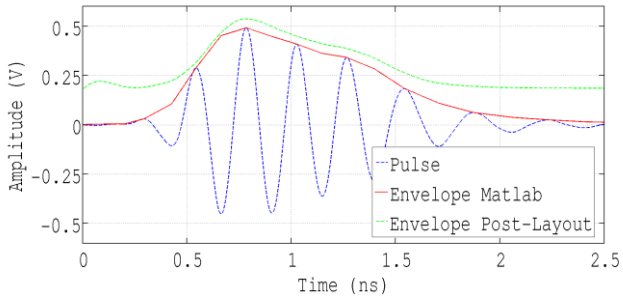

Fig. 8. Extraction of the envelope

The Fig. 9 gives the variations of the delay inside the frequency band. The carrier frequency of the pulse is 3.75 GHz, so according to (8) with k=0, τ should be 66 ps. The delay cell achieves a value of 69 ps at this frequency. A variation of approximately 15% can be observed on the frequency band.

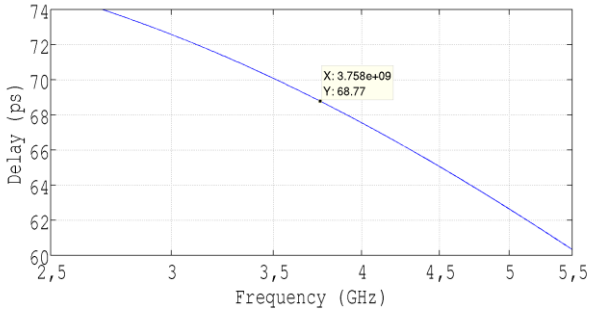

Fig. 9. Variations of the delay inside the frequency band

The instantaneous frequency is given in Fig. 10 after post-layout simulation for the envelope obtained with Matlab and thanks to the full-wave rectifier. In both cases, the result is very similar to the instantaneous frequency from Matlab simulations (Fig. 3). The major differences are still observed at the beginning and during the extinction of the pulse.

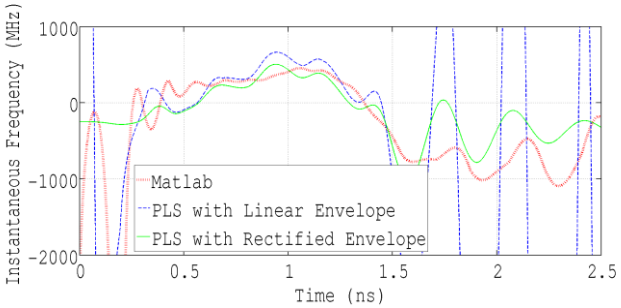

Fig. 10. Comparison between Matlab and post layout simulations for the instantaneous frequency measurement

V. Conclusion

In this paper, a method to measure the instantaneous frequency is applied to an IR-UWB pulse. For that, the design of a full-wave rectifier, an analog delay cell and an analog multiplier is presented from devices of the literature. The combination of these devices shows in post-layout simulation that the on-chip measure of instantaneous frequency in UWB frequency band is feasible and permits to consider new ways for signal analysis in UWB domain.

References

[1] R. Vauche, S. Bourdel, N. Dehaese, J. Gaubert, O. Ramos Sparrow, E. Muhr, and H. Barthelemy, "High efficiency UWB pulse generator for ultra-low-power applications," *Int. J. Microw. Wirel. Technol.*, vol. FirstView, pp. 1–9, Mar. 2015.

[2] F. C. COMMISSION, "Revision of Part 15 of the Commissions Rules Regarding Ultra-Wide-Band Transmission System," *Tech Rep -Docket FCC*, vol. 2–48, 2002.

[3] D. Morche, G. Masson, S. De Rivaz, F. Dehmas, S. Paquelet, A. Bisiaux, O. Fourquin, J. Gaubert, and S. Bourdel, "Double-Quadrature UWB Receiver for Wide-Range Localization Applications With Sub-cm Ranging Precision," *IEEE J. Solid-State Circuits*, vol. 48, no. 10, pp. 2351–2362, Oct. 2013.

[4] M. de Souza, F. e Silva, M. T. de Melo, and L. R. G. S. L. Novo, "Discriminators for Instantaneous Frequency Measurement Subsystem Based on Open-Loop Resonators," *IEEE Trans. Microw. Theory Tech.*, vol. 57, no. 9, pp. 2224–2231, Sep. 2009.

[5] D. Lam, B. Buckley, C. Lonappan, A. Madni, and B. Jalali, "Ultra-wideband instantaneous frequency estimation," *IEEE Instrum. Meas. Mag.*, vol. 18, no. 2, pp. 26–30, Apr. 2015.

[6] R. Vauche, S. Bourdel, N. Dehaese, O. Fourquin, and J. Gaubert, "Fully tunable UWB pulse generator with zero DC power consumption," in *IEEE International Conference on Ultra-Wideband, 2009. ICUWB 2009*, 2009, pp. 418–422.

[7] G.-C. Liang, C.-F. Shih, R. S. Withers, B. F. Cole, and M. E. Johansson, "Space-qualified superconductive digital instantaneous frequency-measurement subsystem," *IEEE Trans. Microw. Theory Tech.*, vol. 44, no. 7, pp. 1289–1299, Jul. 1996.

[8] W. Khalil, B. Bakkaloglu, and S. Kiaei, "A Self-Calibrated On-Chip Phase-Noise Measurement Circuit With -75 dBc Single-Tone Sensitivity at 100 kHz Offset," *IEEE J. Solid-State Circuits*, vol. 42, no. 12, pp. 2758–2765, Dec. 2007.

[9] D. Berthiaume, "Low current, 100 MHz bandwidth envelope detector and characterision of its performances within a 0.18 um CMOS RFID power amplifier implementation at 1.88 GHz",M.S. thesis, University of Québec, Montréal, 2015

[10] S. K. Garakoui, E. A. M. Klumperink, B. Nauta, and F. E. van Vliet, "Compact Cascadable g m -C All-Pass True Time Delay Cell With Reduced Delay Variation Over Frequency," *IEEE J. Solid-State Circuits*, vol. 50, no. 3, pp. 693–703, Mar. 2015.

[11] D. Nicolas, A. Giry, E. Ben Abdallah, S. Bories, G. Tant, T. Parra, C. Delaveaud, P. Vincent, and F. C. W. Po, "SOI CMOS tunable capacitors for RF antenna aperture tuning," 2014, pp. 383–386.

[12] A. N. Saatlo, A. Amiri, and L. Asadpour, "A New CMOS four-quadrant analog multiplier with differential output," 2015, pp. 1–4.